

Supporting Information:

Effect of Viscosity on the Collision Dynamics and Oxidation of Individual Ag Nanoparticles

Donald A. Robinson,[†] Martin A. Edwards,[†] Yuwen Liu,^{†,‡} Hang Ren,[†] and Henry S. White.^{†*}

[†]Department of Chemistry, University of Utah, Salt Lake City, UT 84112, United States

[‡]College of Chemistry and Molecular Sciences, Wuhan University, Wuhan, 430072, China

*Corresponding author: white@chem.utah.edu

Contents

S1. Derivation of the expected cumulative collision count from 1D random walk approximation.....	S-2
S2. 1D random-walk collision frequency: simulation vs analytical solution.....	S-5
S3. Experimental methods	S-6
S4. Examples of experimental <i>i-t</i> traces.....	S-14
S5. Influence of viscosity on nanoparticle transport to microelectrode	S-17
S6. Simulation parameters.....	S-19
S7. Post-processing and analysis of simulated <i>i-t</i> traces.....	S-20
S8. Examples of simulated <i>i-t</i> traces.....	S-21
S9. Analysis methods for measuring <i>i-t</i> peak parameters and cumulative charge vs time from Ag nanoparticle oxidation	S-24
S10. Statistical distributions of <i>i-t</i> peak time parameters from experiment and simulation	S-26
S11. Average number of <i>i-t</i> peaks per particle and peak FWHM.....	S-27
S12. Average cumulative oxidation charge vs time, 10 second time window.....	S-28
S13. References	S-29

S1. Derivation of the expected cumulative collision count from 1D random walk approximation

Consider a nanoparticle initially positioned at a planar electrode surface and undergoing a 1D random walk, as shown in Figure 2. Each time the particle collides with the electrode surface at position, $z = 0$, it does not stick, but instead “reflects” off of the surface to take one step back into solution ($z = \lambda$). By a symmetry argument, the probability of return to the origin at a reflecting barrier (i.e., the electrode surface) after n steps is no different from an unbounded random walk (no reflective barrier). From Figure 2 it is clear that the particle cannot return to its origin at any odd-numbered total of motion steps, n , because any random path beginning at the origin $(0\lambda, 0\tau)$ will end up at an odd distance from the electrode on these time-steps, making $z = 0\lambda$ (electrode collision) impossible. The probability of return to the origin after n steps is thus

$$P_0(n) = 0 \quad \text{if } n \text{ is odd} \quad (\text{S1})$$

$$P_0(n) = \frac{1}{2^n} C_{n/2}^n \quad \text{if } n \text{ is even}$$

where C_k^m in eq S1 is the binomial coefficient (eq S2)

$$C_k^m = \frac{m!}{(k)!(m-k)!} \quad (\text{S2})$$

The expected number of collisions, N_c , is given by the following recurrence relation.

$$N_c(n) = N_c(n-1) + P_0(n) \quad (\text{S3})$$

Thus we can say

$$N_c(n) = N_c(0) + \sum_{i=1}^n P_0(i) \quad (\text{S4})$$

If we count the particle at the electrode surface at $n = 0$ as the very first electrode collision, then $N_c(0) = 1$. Because the odd terms of this sum are all equal to 0, we reformulate the sum over only the even terms and substitute $N_c(0) = 1$ and eq S1 into eq S4 to give eq S5.

$$N_c(2n) = 1 + \sum_{i=1}^n \frac{1}{2^{2i}} C_i^{2i} \quad (\text{S5})$$

After substituting the factorial form of C_i^{2i} (from eq S2), we obtain

$$N_c(2n) = 1 + \sum_{i=1}^n \frac{1}{2^{2i}} \frac{(2i)!}{i!i!} \quad (\text{S6})$$

The largest time step in our simulations, τ_{\max} , is 6.4 ns. ($\tau_{\max} = \tau_o$ for a 35 nm radius particle in aqueous solution, see Table S2 below). Our sampling interval in the simulations, Δt_s , is 20 μ s, similar to experiment. Thus, the minimum number of motion steps possible in our simulations for any sampling interval is $\Delta t_s / \tau_{\max} = 3125$ steps. Because our first sampled N_c value occurs after a large number of steps ($n \geq 3125$), we apply Stirling's approximation, $i! \approx \sqrt{2\pi i} (i/e)^i$, to the factorials in eq S6 to give eq S7.

$$N_c(2n) \approx 1 + \sum_{i=1}^n \frac{1}{\sqrt{\pi i}} + C \quad (\text{S7})$$

Here, C represents the cumulative error in the Sterling approximation for small i . The summation of $i^{-1/2}$ from 1 to n is approximately equal to $2n^{1/2}$, leading to eq S8

$$N_c(2n) \approx 2\sqrt{\frac{n}{\pi}} + C' \quad (\text{S8})$$

where C' incorporates errors in this approximation, the addition of '1' and C . We approximate $C' \approx 0$, which introduces very little error, as can be seen by comparison of the numerical solution of $N_c(t)$ with eq S9 shown in Figure S1a.

$$N_c(n) \approx \sqrt{\frac{2n}{\pi}} \quad (\text{S9})$$

Note, in eq 9, we are able to include odd terms without introducing any significant error due to $P_0(n)$ being small for large n . We use eq S9 (eq 11 in the main text) as the expected cumulative collision count throughout this work.

S2. 1D random-walk collision counts and frequency: simulation vs analytical solution

Figure S1 shows the values for the particle collision count and frequency as a function of time (35 nm radius particle). In Figure S1a, comparison of the numerical (dashed line) and values from eq S9/11 (solid line) shows that the error, C' , included in eq S8 is minimal and can be well approximated as zero.

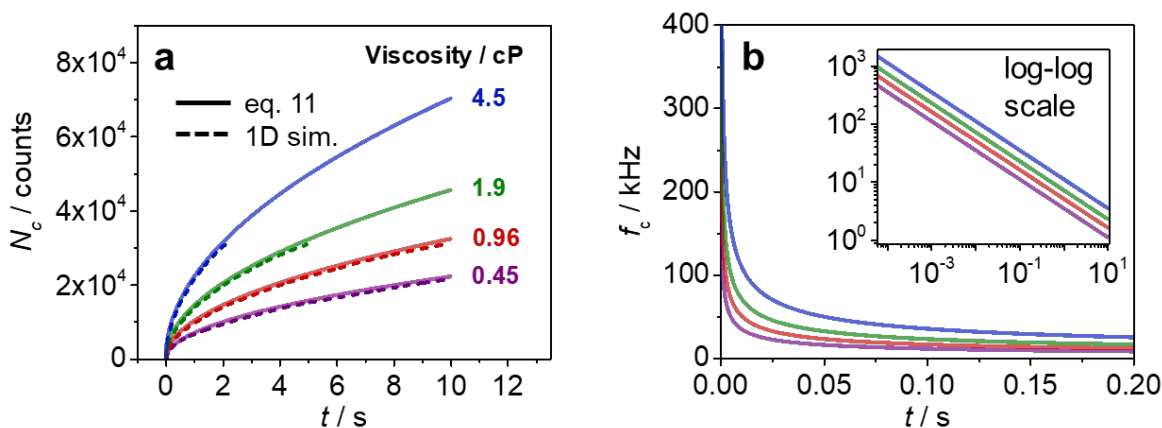


Figure S1. One-dimensional approximation of the average **a)** cumulative collision count, N_c (eq S9/11), and **b)** collision frequency, f_c (eq 12), as a function of t , following the first collision. The averaged N_c of 1000 individual random-walk simulations are included as a dashed line in part a).

S3. Experimental methods

Materials

Water was purified using a Smart2Pure 12 UV/UF water purification system (Thermoscientific, Barnstead), giving a resistivity of 18.2 M Ω ·cm. Citrate-stabilized Ag nanoparticles of quasispherical shape, 71 \pm 8 nm diameter, referred to in the main text as 35 nm-radius Ag nanoparticles, were purchased from nanoComposix, Inc. The stock solution contained \sim 0.91 nM Ag nanoparticles (\sim 5.5 \times 10¹¹ particles/mL) in 2 mM sodium citrate buffer, pH 7.5. Trisodium citrate dihydrate (Na₃Citrate) and glycerol were obtained from Fisher Scientific. 1,1'-Ferrocenedimethanol and potassium nitrate (KNO₃) were purchased from Sigma-Aldrich.

Electrode cleaning protocol

Prior to performing a Ag nanoparticle collision measurement, a 12.5 μ m diameter Au microdisk working electrode (CH Instruments) was polished with Microcut® paper discs, 1200 grit (Buehler, ITW, Inc), then rinsed with water and subsequently polished on a diamond lapping sheet, 0.02 μ m grit size (LFCF, Thorlabs, Inc) and rinsed again with water. The Au microelectrode was then cycled in 0.1 M HClO₄ from -0.8 to 1.2 V vs a Hg/HgSO₄ reference electrode (sat K₂SO₄, CH Instruments) at a scan rate of 100 mV/s until a reproducible voltammogram was obtained. Figure S2 shows a representative cyclic voltammogram (CV) for the last cleaning cycle. The two anodic peaks at ca. 0.65 and 0.85 V are due to the formation of Au surface oxides and the final anodic onset at ca. 1.1 V is attributed to water oxidation. The cathodic peak at ca. 0.4 V on the reverse scan arises from the reduction of Au oxide. The cathodic wave from -0.25 to -0.80 V corresponds to oxygen reduction (no purging gas was used). If after 30 cycles the cathodic peak at 0.4 V did not reach at least -4.5 nA, then the electrode was mechanically polished again and

recycled in 0.1 M HClO₄ until the target CV response in Figure S2 was obtained. The cycling was terminated at 0 V on the negative potential sweep after the Au oxide reduction peak. The microelectrode was rinsed thoroughly before performing Ag nanoparticle collision measurements.

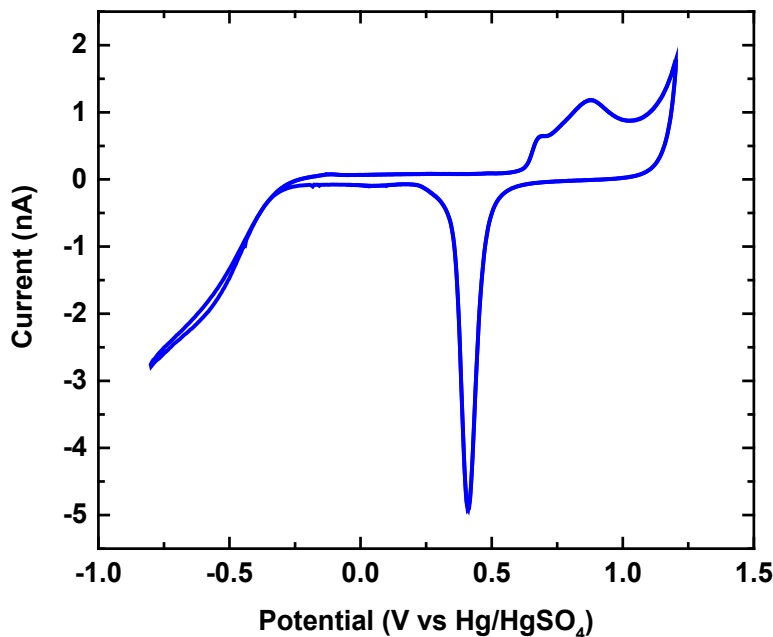


Figure S2. Representative cyclic voltammogram of a 6.25 μm radius Au microdisk electrode in 0.1 M HClO₄ at a scan rate of 100 mV/s.

Viscosity measurements

Solutions containing 20 mM KNO₃ and 6 mM Na₃Citrate were prepared using water and mixed glycerol-water solvents (20% and 40% glycerol by volume). Solution densities were measured in triplicate weighing 1 mL of solution. The kinematic viscosities of each solution were measured in triplicate with a Cannon-Fenske viscometer tube (constant: ~ 0.015 centistokes per second). Table S1 lists the measured densities. We assume that the dilute Ag nanoparticle concentrations used in this study have negligible effect on the solution viscosity.

Table S1. Measured viscosity in glycerol-water solutions

% Glycerol % by volume	ρ_{sol} g/mL	μ cSt	η cP	η_{p} cP
0	0.987 ±0.004	0.970 ±0.008	0.958 ±0.009	0.957
20	1.048 ±0.001	1.808 ±0.006	1.895 ±0.003	1.876
40	1.103 ±0.007	4.091 ±0.007	4.511 ±0.006	4.484

$T = 22 \pm 1$ °C; ρ_{sol} , measured solution density; μ , measured kinematic viscosity; η , measured dynamic viscosity; η_{p} , dynamic viscosity predicted by Cheng's formula;¹ cSt, centistokes; cP, centipoise. All glycerol-water mixtures contained 20 mM KNO₃ and 6 mM Na₃Citrate.

Preparation of Ag nanoparticle sample solutions

Ag nanoparticle suspensions were prepared using the same mixed solvents (0%, 20%, and 40% glycerol by volume) and electrolyte concentrations (20 mM KNO₃ + 6 mM Na₃Citrate) as reported in the section above. For example, in the preparation of the 9 pM Ag nanoparticle suspension in 40% glycerol, a 10 μ L aliquot of the 0.91 nM stock Ag nanoparticle suspension was added to a mixture containing 20 μ L of 1.0 M KNO₃, 60 μ L of 0.1 M Na₃Citrate, 510 μ L of water, and 400 μ L of glycerol. The suspension was gently swirled/shaken for a few seconds to achieve a homogeneous mixture. No visible evidence of nanoparticle aggregation²⁻⁵ was observed for more concentrated samples (20 pM Ag nanoparticles) on the time scale of the measurement.⁵

Electrochemical measurements

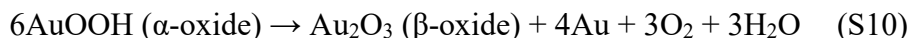
Chronoamperometric collision/oxidation measurements were performed within 2 min. of preparing a Ag nanoparticle solution using a 12.5 μ m diameter Au disk working electrode held at 0.5 V vs a chloridized Ag wire quasireference (QRE) electrode. A Pine bipotentiostat (Model AFRDE5) provided the voltage input to a Chem-Clamp amplifier (Dagan Corporation). The 3-

pole low-pass Bessel filter on the Chem-Clamp was set to 10 kHz. Data were acquired at a 50 kHz sampling rate using a PCI-6251 data acquisition card (National Instruments) and custom written LabVIEW software.

Au microelectrode activation protocol

Even after thorough cleaning by the protocol described above, many experiments failed to produce *i-t* peaks. Thus, an *in situ* electrode activation protocol was developed to significantly improve reproducibility.

Figure S3a shows the CV of the Au microelectrode in a typical electrolyte used for nanoparticle collision measurements. At 0 V vs the QRE, no surface oxides exist on Au. The anodic Au oxide formation region occurs from 0.4 to 0.7 V on the positive scan and the subsequent reduction of Au oxide takes place from 0.2 to 0 V on the reverse scan. The cathodic onset for oxidation of water occurs at ca. 0.8 V. According to the study of Koper and coworkers,⁶ an important surface structural transformation occurs before oxygen is evolved as the final product through the oxidation of water. The authors proposed a Au oxide decomposition pathway as the last step in the oxygen evolution reaction (OER). It was suggested that after forming 3 monolayers of hydrous Au oxide, O₂ is finally evolved through the transformation of AuOOH to Au₂O₃ and metallic Au according to eq S10.⁶



Such a transformation is likely to have a dramatic effect on the Au surface structure before and after the Au₂O₃ is reduced on the reverse sweep. The method of surface restructuring by electrochemical oxidation of Au to Au oxide and subsequent reduction back to Au has been demonstrated to produce highly active electrocatalysts for CO₂ and O₂ reduction that outperform

polycrystalline Au and Au nanocrystals of various controlled morphologies.⁷⁻⁸ It is hypothesized that the so-called “oxide-derived Au” has enhanced activity because of an increased density of partially oxidized surface terminations at grain boundaries that become kinetically trapped after the electroreduction of Au₂O₃.⁸ The following potential step experiments show that this electrochemical activation method also helps to improve the ensemble electrooxidation rate of citrate-capped Ag nanoparticles suspended in solution.

The top panel of Figure S3b shows the potential step waveform applied and the bottom trace shows the resulting chronoamperometric response in the presence of 9 pM Ag nanoparticles. This experiment was performed immediately after the electrode cleaning protocol as described in the previous section. The potentials applied in the experiment are 0.0, 0.5, and 1.0 V vs Ag/AgCl QRE, respectively, which corresponds to -0.3, 0.2, and 0.7 V vs the standard electrode potential for the Ag/Ag⁺ redox couple ($E^0 = 0.8$ V vs SHE).⁹ As shown in Figure S3b, at $t = 30$ s (Step 1), the electrode potential is stepped to 0.5 V, a potential that has been reported to result in observable current transients that signal the electrode collision and electrodisolution of Ag nanoparticles.⁵ However, just one amperometric event signal is barely visible above the noise in the 2 minutes that follow for Step 1. This measurement represents a poor experimental outcome because the expected rate of nanoparticle arrival, R_{NP} , should be on the same order of magnitude as that calculated by eq S11.⁵

$$R_{NP} = 4Dc_{NP}a \quad (\text{S11})$$

Here, c_{NP} is the concentration in nanoparticles per unit volume (5.5×10^9 nanoparticles cm^{-3} for Figure S3b) and a is the radius of the microelectrode (6.25 μm). The Ag nanoparticle diffusion

coefficient, D , is calculated as $6.4 \times 10^{-8} \text{ cm}^2 \text{ s}^{-1}$ according to the Stokes-Einstein equation (eq 2 in the main text). The predicted value of R_{NP} is $0.87 \text{ nanoparticles s}^{-1}$, as calculated by eq S11.

In step 2 of Figure S3b, the potential is stepped to 1.0 V for 30 s. The resulting amperometric response shows a rapid frequency of current transient peaks ($\sim 3 \text{ nanoparticles s}^{-1}$, roughly 3-fold faster than predicted above assuming steady-state diffusive flux) and a baseline current that decays over the 30 s period from 4 to 2 nA, which is more easily seen in the blow up trace (Figure S3c). The initial baseline current (4 nA) is high in comparison that shown at 1.0 V in the CV of Figure S3a (1.5 nA), indicating that electrocatalytic water oxidation is occurring not only at the Au electrode, but also at the partially oxidized Ag nanoparticles adsorbed on Au electrode. We thus infer that the $i-t$ events shown for all 1.0 V steps marked in blue (steps 2, 5, and 10) result from the simultaneous contributions of both direct Ag nanoparticle oxidation/dissolution and electrocatalytic water oxidation at the partially oxidized Ag nanoparticles, as reported by Zhang and coworkers.¹⁰ In step 3, the potential is stepped negative to 0.0 V for 30 s, thus reducing the Au oxides back to Au^0 . In step 4, the potential is returned to 0.5 V and held there for $\sim 100 \text{ s}$, resulting in a collision rate of roughly 0.1-0.2 nanoparticles per second, within one order of magnitude of the predicted rate ($0.87 \text{ nanoparticles s}^{-1}$); see part d for a zoomed in view of the current in this region.

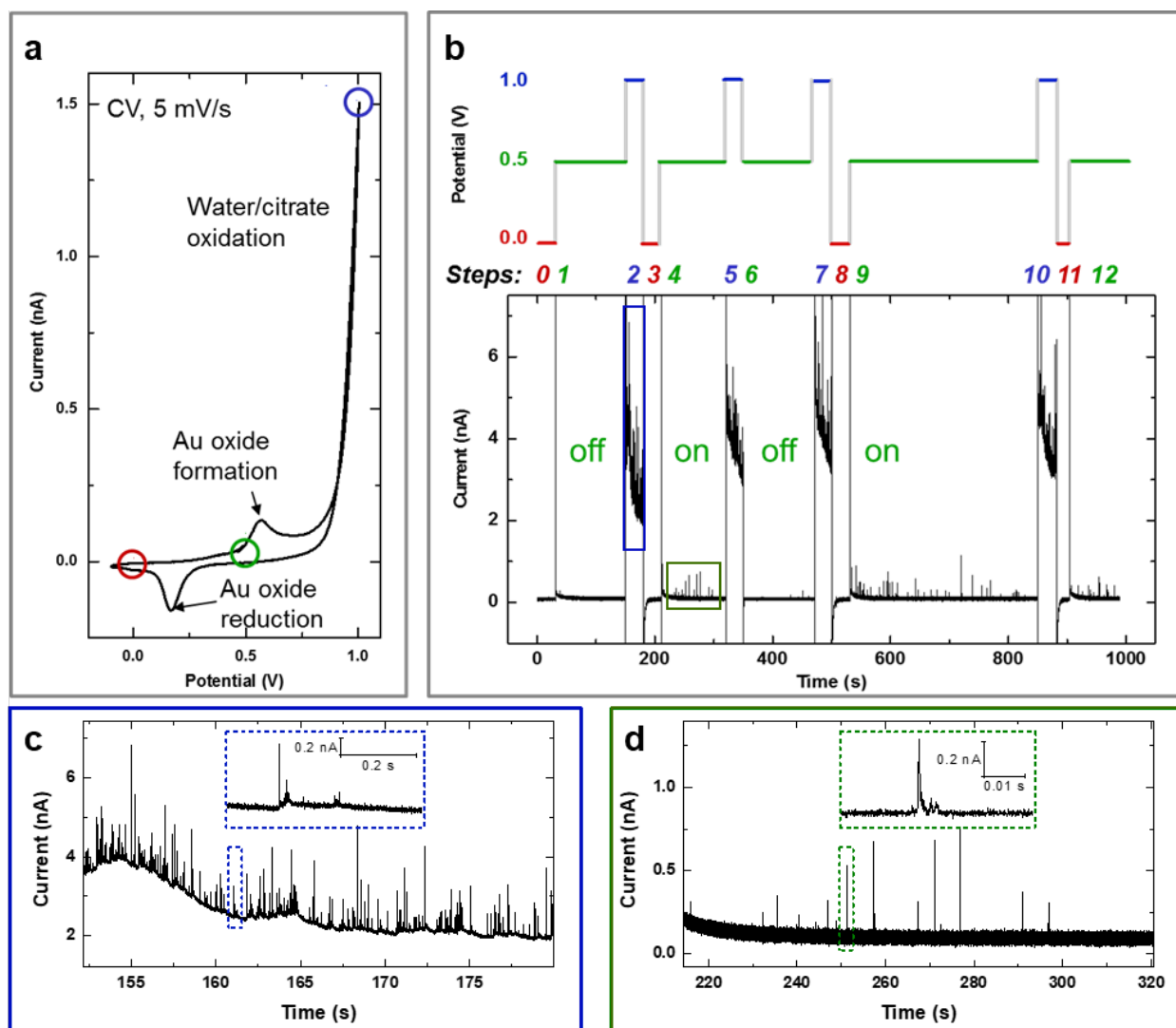


Figure S3. (a) Cyclic voltammetry of Au oxide formation and reduction on a 6.25 μm radius Au microdisk electrode in 6 mM $\text{Na}_3\text{Citrate}$ + 20 mM KNO_3 at a scan rate of 5 mV/s, potential vs Ag/AgCl QRE. The Au oxide formation/reduction peaks are labeled on the plot. Red, green, and blue circles correspond to the potentials used for the electrode activation experiment in part b. (b) Potential step experiment demonstrating activation and deactivation of the Au electrode surface for reporting Ag nanoparticle electrodisolution events using 9 pM Ag nanoparticles in 6 mM $\text{Na}_3\text{Citrate}$ + 20 mM KNO_3 . The potential step waveform is shown on the top panel and corresponding chronoamperometric trace is shown below. Each potential step is labeled with integers according to step order and color-coded to the potential applied, vs Ag/AgCl QRE. Expanded view of i - t traces corresponding to (c) potential step 2 (1.0 V) and (d) potential step 4 (0.5 V) in part b, insets show enlarged views of oxidation current from single-nanoparticle events.

The lower-than-predicted rate is thought to occur because some collisions may not result in an observable oxidation current, due to fast mass transport of trace organic contaminants in solution to the microelectrode. Also, considering the relatively low electrolyte concentration (low solution conductivity), we previously estimated that the Ag nanoparticle must collide at least 16 times with the electrode to charge 99% of its double-layer.¹¹ Some nanoparticles may only collide a few times and thus only partially charge the double-layer, such that the current is not observable above the noise.

Interestingly, as shown in steps 5-6 of Figure S3b, if the potential is stepped to 1.0 V and returned to 0.5 V without first reducing the Au oxides at 0 V, the resulting *i-t* peak frequency is significantly lower than that of step 4. We infer that the Au oxide structure generated at 1.0 V acts to prevent sufficient electrical contact with the colliding Ag nanoparticles. The step sequence, 7-8-9, follows the same sequence as 2-3-4, showing that *i-t* events resulting from Ag nanoparticle oxidation can again be recovered. In a typical experiment, this electrode treatment is applied in between acquisitions of amperometric traces of 200 s or longer at 0.5 V.

S4. Examples of experimental i - t traces

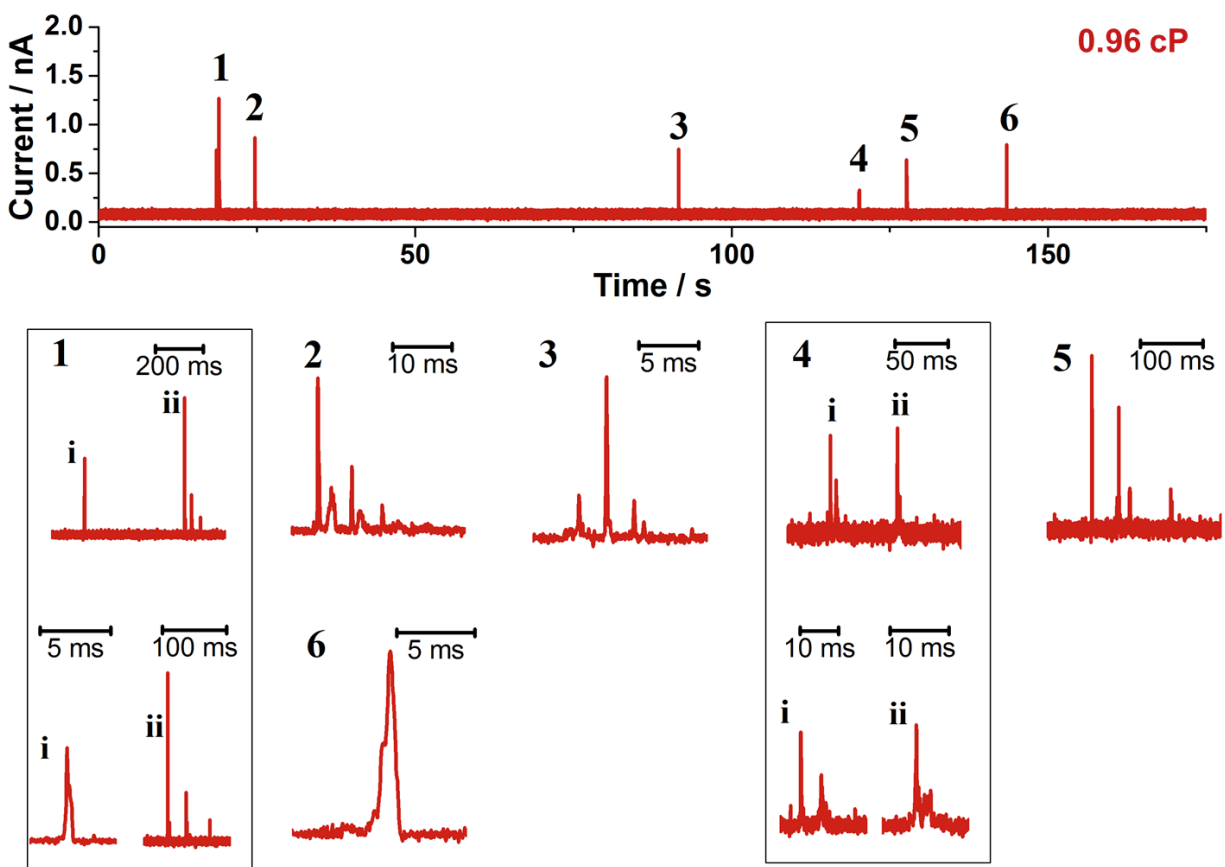


Figure S4. Experimental i - t trace resulting from oxidations of 35 nm-radius Ag nanoparticles in aqueous solution ($\eta = 0.96$ cP) containing 20 mM KNO_3 , 6 mM trisodium citrate. Arabic numerals label individual nanoparticle oxidation events. Roman numerals identify expanded portions of the multiplexed i - t response in the panels below, which use different time scales (as indicated). These represent replicate measurements of those shown in Figure 3a.

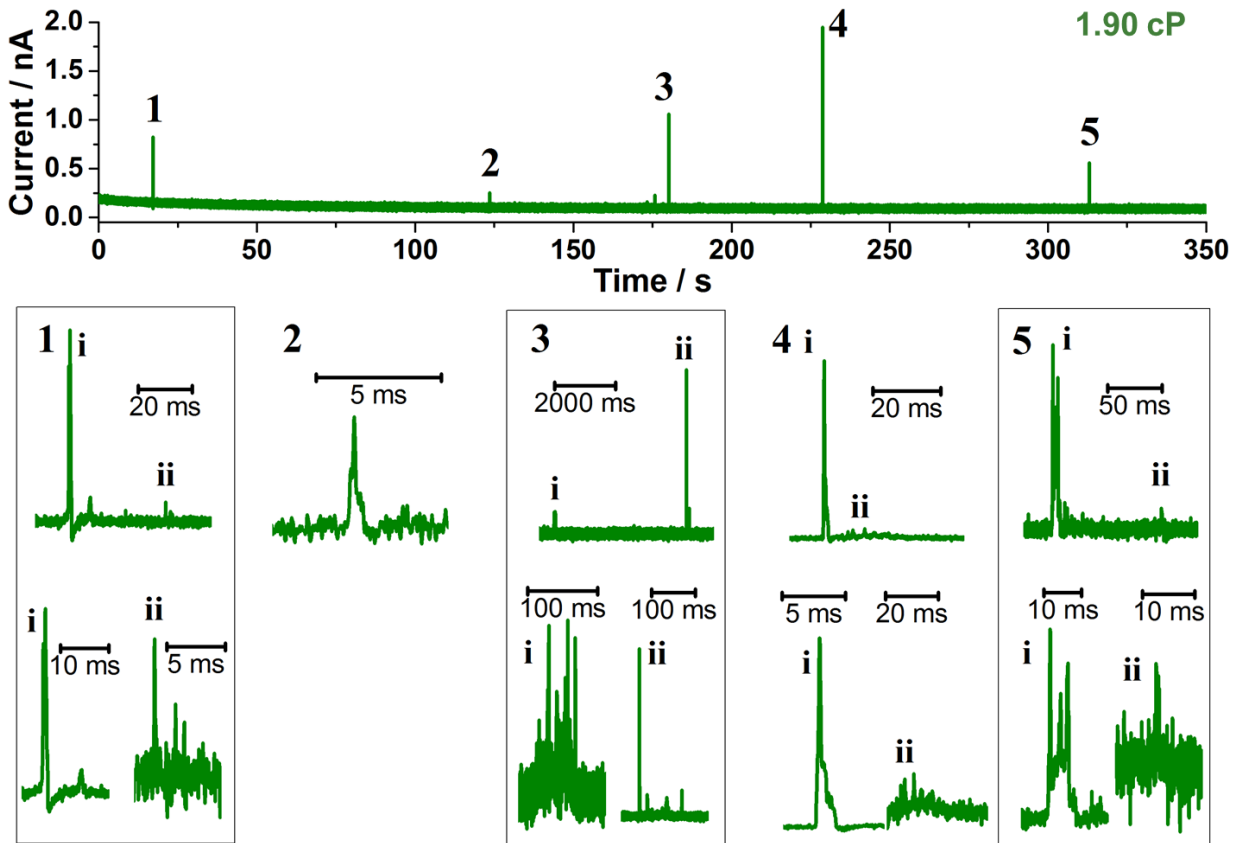


Figure S5. Experimental i - t trace resulting from oxidations of 35 nm-radius Ag nanoparticles in 20% glycerol by volume solvent ($\eta = 1.90$ cP) containing 20 mM KNO_3 , 6 mM trisodium citrate. Arabic numerals label individual nanoparticle oxidation events. Roman numerals identify expanded portions of the multiplexed i - t response in the panels below, which use different time scales (as indicated).

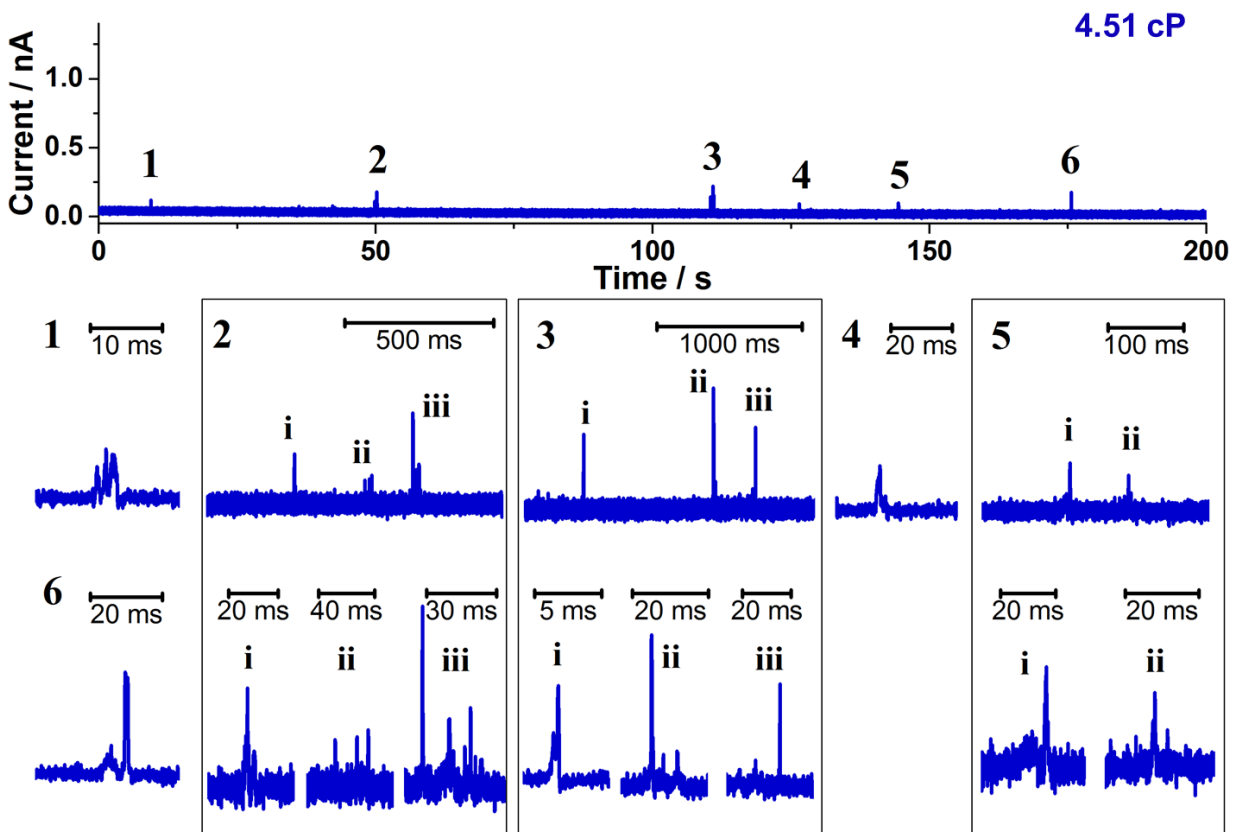


Figure S6. Experimental $i-t$ trace resulting from oxidations of 35 nm-radius Ag nanoparticles in 40% glycerol by volume solvent ($\eta = 4.51$ cP) containing 20 mM KNO_3 , 6 mM trisodium citrate. Arabic numerals label individual nanoparticle oxidation events. Roman numerals identify expanded portions of the multippeak $i-t$ response in the panels below. These represent replicate measurements of those shown in Figure 3b.

S5. Influence of viscosity on nanoparticle transport to a microelectrode

As mentioned in section S3, the steady-state rate of nanoparticle transport to the electrode, R_{NP} , is $4Dc_{\text{NP}}a$, (eq S11). We write a more general form of eq S11 by considering a nanoparticle arrival rate, R_{NP} (in units of nanoparticles per second), normalized by the electrode area, $A_{\text{el}} = \pi a^2$, and nanoparticle number concentration, c_{NP} (nanoparticles per unit volume), to give the nanoparticle-transfer coefficient, μ_{NP} .

$$\mu_{\text{NP}} = \frac{R_{\text{NP}}}{A_{\text{el}}c_{\text{NP}}} \quad (\text{S12})$$

The formula to predict μ_{NP} at an inlaid disk microelectrode, based on Fick's laws of diffusion, is given by eq S13.⁹

$$\mu_{\text{NP}} = \frac{4D}{\pi a} \quad (\text{S13})$$

After substituting in $D = k_{\text{B}}T/6\pi\eta r$ via the Stokes-Einstein (eq 3 in main text), the mass transfer coefficient can then be represented as a function of solution viscosity.

$$\mu_{\text{NP}} = \frac{2k_{\text{B}}T}{3\pi^2\eta ra} \quad (\text{S14})$$

Figure S7 shows the experimentally determined μ_{NP} calculated from the measured R_{NP} (eq S12), as a function of η^{-1} , giving the expected linear relationship following eq S14. The slope of the theoretical curve calculated by eq S14 is roughly 2.5 times steeper than the experimental slope. A possible explanation for the discrepancy between theory and experiment in nanoparticle transport rates is discussed in section S3.

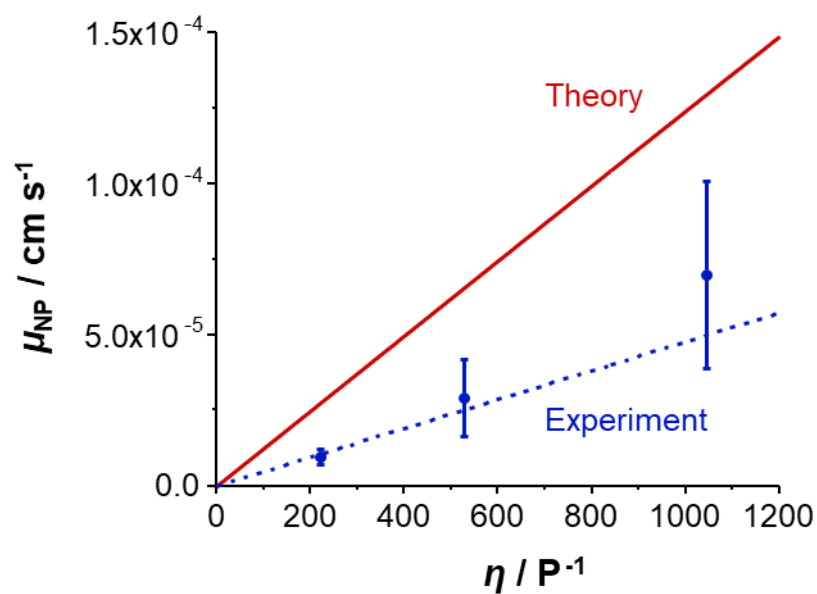


Figure S7. Comparison of experimentally determined nanoparticle-transfer coefficient based on measurements of R_{NP} over 200 s time increments. Error bars represent standard deviation from 5 replicate measurements of R_{NP} for each viscosity. Experimentally measured R_{NP} was normalized by A_{el} and c_{NP} according to eq S12. Theoretical curve was calculated using eq S14.

S6. Simulation parameters

Table S2. Simulation parameters

j_c	T	r_0	η	D_0	τ_0	λ_0
A cm ⁻²	K	nm	cP	$\times 10^{-8}$ cm ² /s	ns	nm
400	295	35.4	0.96	6.4	6.1	0.28
400	295	35.4	1.90	3.2	3.1	0.14
400	295	35.4	4.51	1.4	1.3	0.06

r_0 , initial nanoparticle radius; D_0 , initial simulation diffusion coefficient calculated from eq 3 with $T = 295$ K; τ_0 , initial simulation step time calculated from eq 7; λ_0 , initial simulation step distance calculated from eq 6.

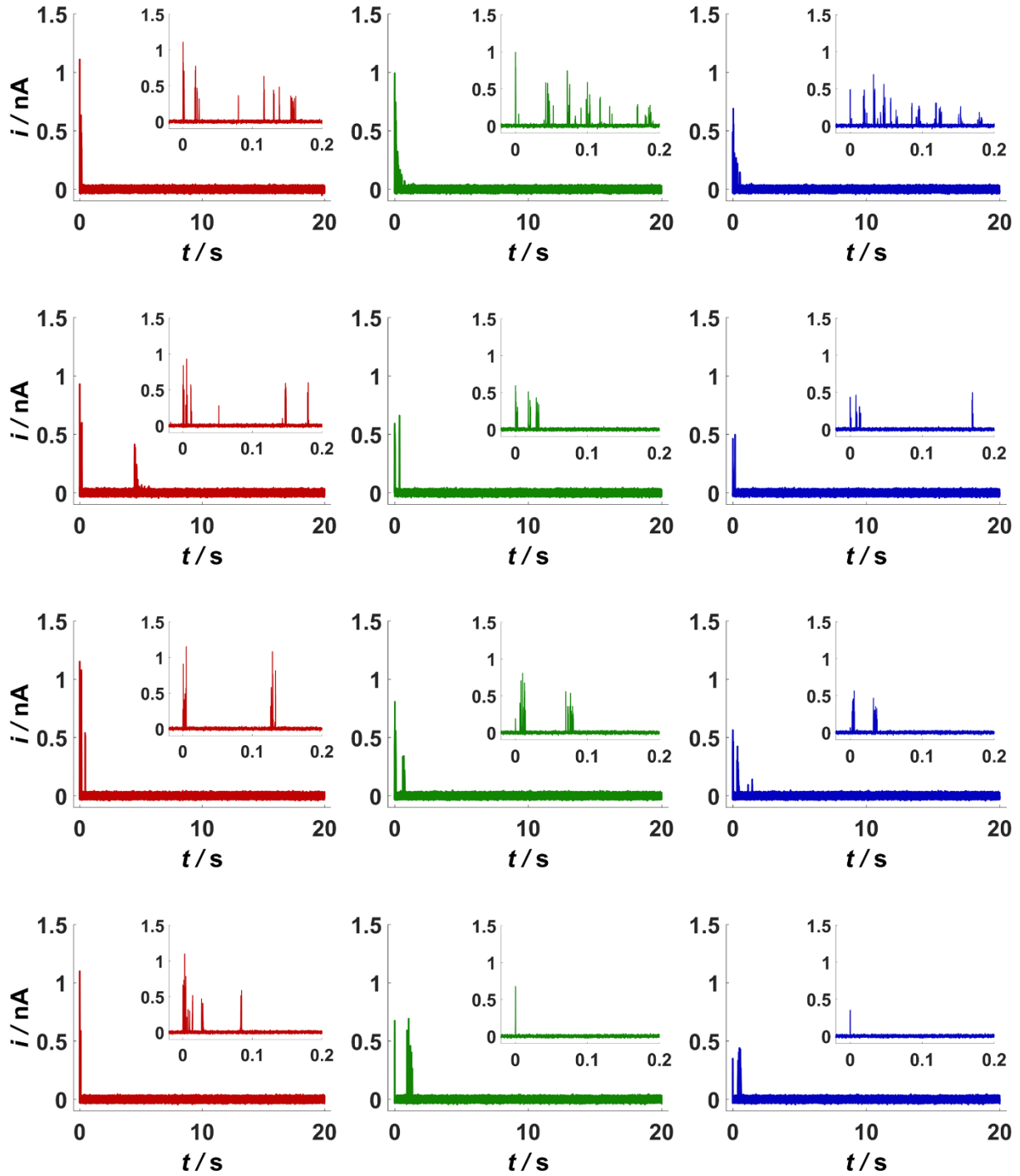
S7. Post-processing and analysis of simulated $i-t$ traces

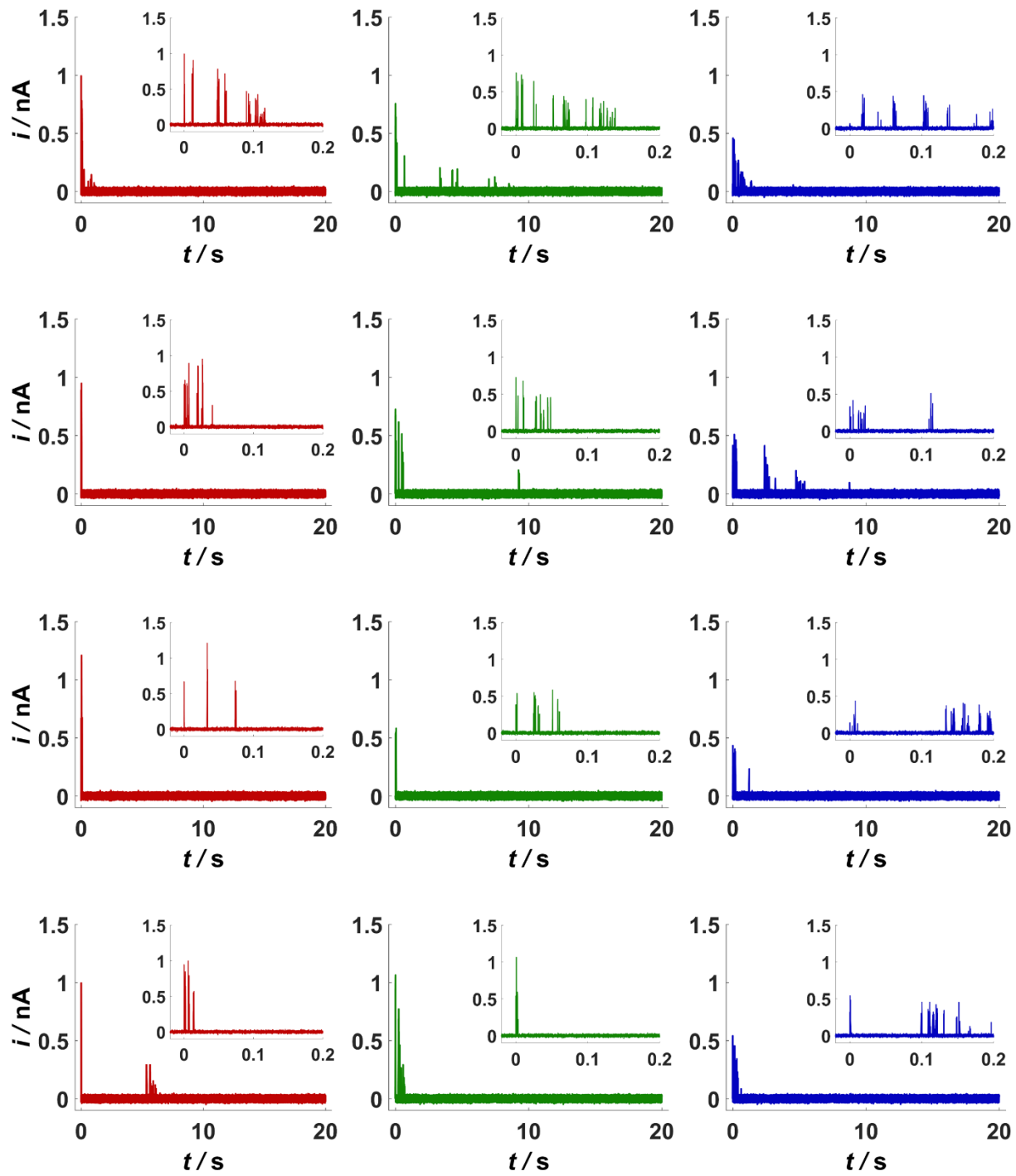
In order to provide a better comparison to experimentally acquired $i-t$ traces, simulated noise was added prior to peak analysis. Simulated $i-t$ traces were originally sampled at 250 kHz, a factor of five higher sampling than the experimental acquisitions. A baseline zero current was appended to each $i-t$ trace from $t = -20 \mu\text{s}$ to $t = 20 \mu\text{s}$; (this was done only for artistic preference because there is always baseline current in the time preceding the first peak event in experimental $i-t$ traces). Gaussian noise with standard deviation of 50 pA was added to each simulated trace; this noise level is a factor of 5 times higher than that measured for the experimental $i-t$ traces acquired at 50 kHz sampling (10 pA standard deviation of the noise for experiment). Next, a 3-pole Bessel filter function was applied to the noisy simulated traces with a low-pass filter cutoff frequency of 10 kHz, similar to experimental filter. The resulting traces were then down-sampled from 250 kHz to 50 kHz, which produced the final simulated currents comparable to experimentally observed amperometric traces, with a noise standard deviation of ~ 10 pA.

The fully processed simulated $i-t$ traces were analyzed in MATLAB. For analysis of i_p and t_p data, the “findpeaks” function of MATLAB was utilized with a minimum peak height cutoff of 50 pA (a factor of ~ 5 times greater than standard deviation of the noise), a minimum peak width of 30 μs , and a minimum peak threshold of 10 pA.

Peak integration was performed on the final post-processed simulated $i-t$ traces using a trapezoidal numerical integration function in MATLAB. In order to be comparable with the integration of experimental $i-t$ peaks, the charge arising from $i-t$ peaks less than 50 pA were not included in the analysis. The resulting $Q-t$ curves for each simulated nanoparticle were averaged together to give the average cumulative charge vs time functions shown in Figure 7a of the main text.

S8. Examples of simulated i - t traces





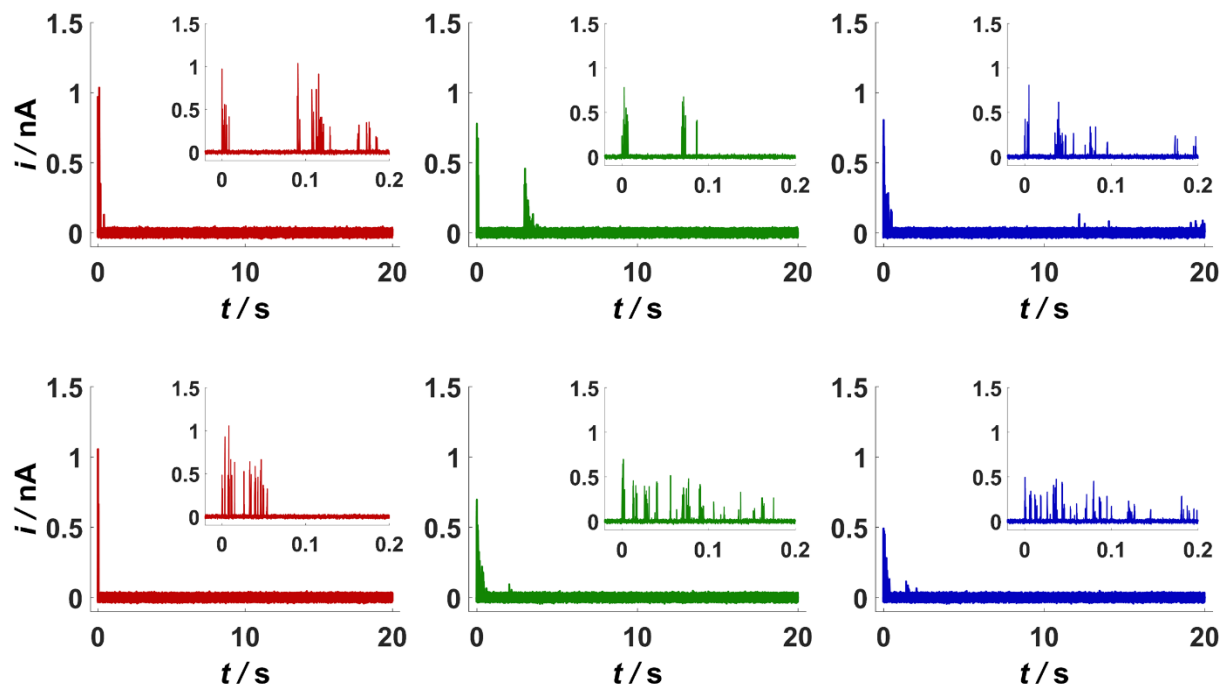


Figure S8. Simulated i - t traces resulting from oxidations of 35 nm-radius Ag nanoparticles over a total time of 20 s with 3 different solution viscosities: 0.96 cP (red), 1.90 cP (green), and 4.51 cP (blue). Ten examples out of one-hundred single-nanoparticle simulations are shown for each of the three viscosities. Each row of horizontally aligned traces corresponds to independently simulated nanoparticles that begin their random walks at exactly the same x-y position at the electrode surface. Inset traces show the current responses during the first 200 ms.

S9. Analysis methods for measuring i - t peak parameters and cumulative charge vs time from Ag nanoparticle oxidation

All experimental i - t traces were analyzed using the “peak analysis dialogue” function of Origin 9.1, as shown in Figure S9. First an individual Ag nanoparticle oxidation event is selected for analysis (blue asterisk in Figure S9a, expanded view shown in Figure S9b). Figure S9c shows expanded sections of S9b where one can see the addition of the charge from each peak (green triangles) as a step increase in charge in the blue Q - t curve. Time gaps between peaks were excluded from the integration and consequently show no slope in the Q - t curve. All peak currents, i_p , and corresponding times were analyzed for each viscosity were combined into two data columns, x-column for peak time and y-column for i_p , excluding those in which $i_p < 50$ pA, and then plotted as a scatter in Figure 5b of the main text. All individual i - t peak areas (Q_p) and corresponding peak times were imported into MATLAB, organized as one dataset for each single-nanoparticle event (the number of Q_p values per nanoparticle are contingent on how many peaks were observed for each single-nanoparticle multippeak i - t event). A custom-written cumulative moving average function was applied to the Q_p vs peak time data for each of the three viscosities to give the three experimental Q - t curves shown in Figure 7a.

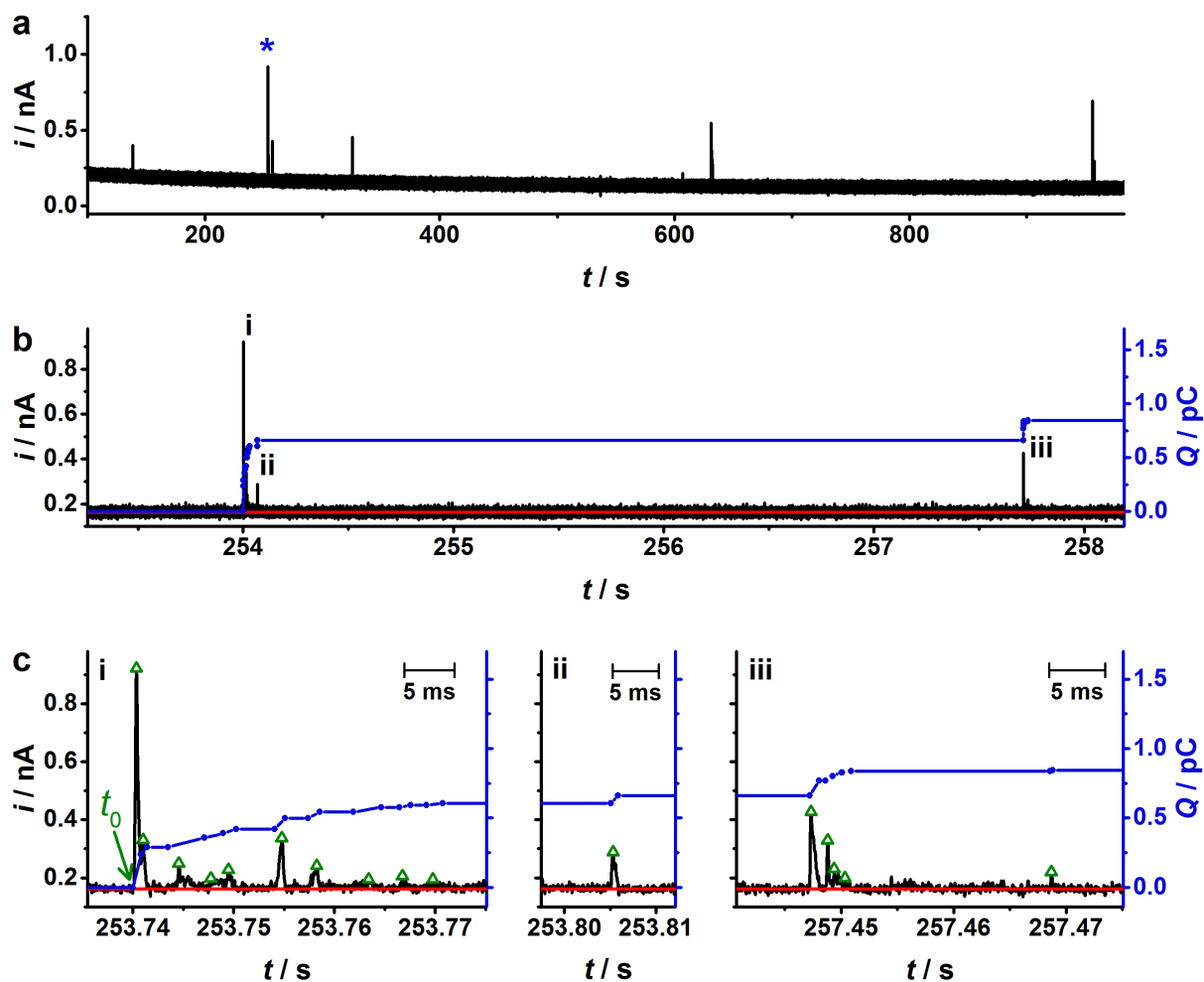


Figure S9. Analysis of an example multiplexed i - t cluster resulting from oxidation of an individual Ag nanoparticle in 40% glycerol (20 mM KNO_3 , 6 mM $\text{Na}_3\text{Citrate}$). **a)** Chronoamperometric trace showing 5 individual nanoparticle oxidation events; the blue asterisk labels an event with a total duration of ~ 3.7 s; **b)** corresponding expanded view of the multiplexed i - t cluster with Roman numerals labelling three particular sections; **c)** three detailed expanded sections of the i - t cluster: each section contains peak currents, times (i_p , t_p) labelled with green triangles, baseline for peak integration shown by red horizontal line, and stepwise integration of each i - t peak event (blue scatter/line plot, shown as a cumulative sum of the charge, Q). Time of first collision labelled as t_0 .

S10. Statistical distributions of i - t peak time parameters from experiment and simulation

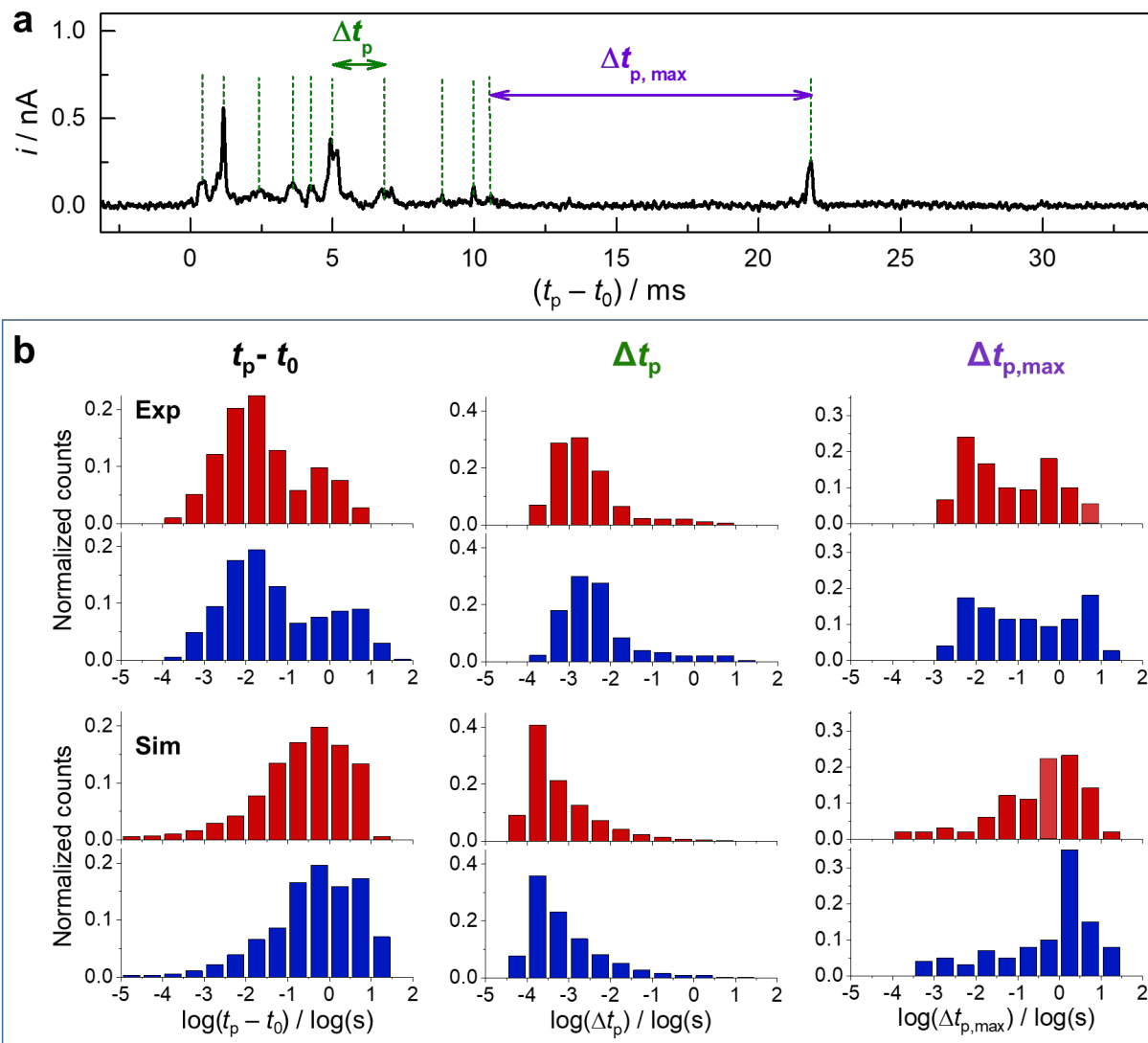


Figure S10. **a)** Example experimental multipeak i - t trace for a single Ag nanoparticle oxidation event in 0% glycerol (0.96 cP) with labels defining the interpeak duration (Δt_p) and the maximum interpeak duration ($\Delta t_{p, \max}$). **b)** Histograms of $\log_{10}(t_p - t_0)$, $\log_{10}(\Delta t_p)$, and $\log_{10}(\Delta t_{p, \max})$ for experimental results (top panels) and simulation results (bottom panels) acquired for 0% glycerol, 0.96 cP (red) and 40% glycerol, 4.51 cP (blue), all vertical axes are normalized by total counts. Experimentally measured $\Delta t_{p, \max}$ distribution was acquired from multipeak i - t clusters of 150 individual Ag nanoparticles. Histograms of simulations were constructed from 100 individual 20 s nanoparticle random walks for each viscosity.

S11. Average number of *i-t* peaks per particle and peak FWHM**Table S3.** Average peak count per nanoparticle and peak half-widths.

η cP	N_{NP}	Peak Number ($\pm\sigma$) counts per nanoparticle	FWHM ($\pm\text{SE}$) μs
Experiment			
0.96	155	8 (± 6)	292 (± 7)
1.9	165	8 (± 7)	303 (± 7)
4.51	168	7 (± 6)	302 (± 8)
Simulation			
0.96	100	66 (± 4)	50.8 (± 0.2)
1.9	100	80 (± 4)	51.7 (± 0.2)
4.51	100	92 (± 5)	53.4 (± 0.2)

N_{NP} , number of nanoparticles analyzed; FWHM, full-width-at-half-maximum; $\pm\sigma$, standard deviation; $\pm\text{SE}$, standard error of mean, $\text{SE} = \sigma/(N_{\text{NP}}^{0.5})$.

S12. Average cumulative oxidation charge vs time, 10 second time window

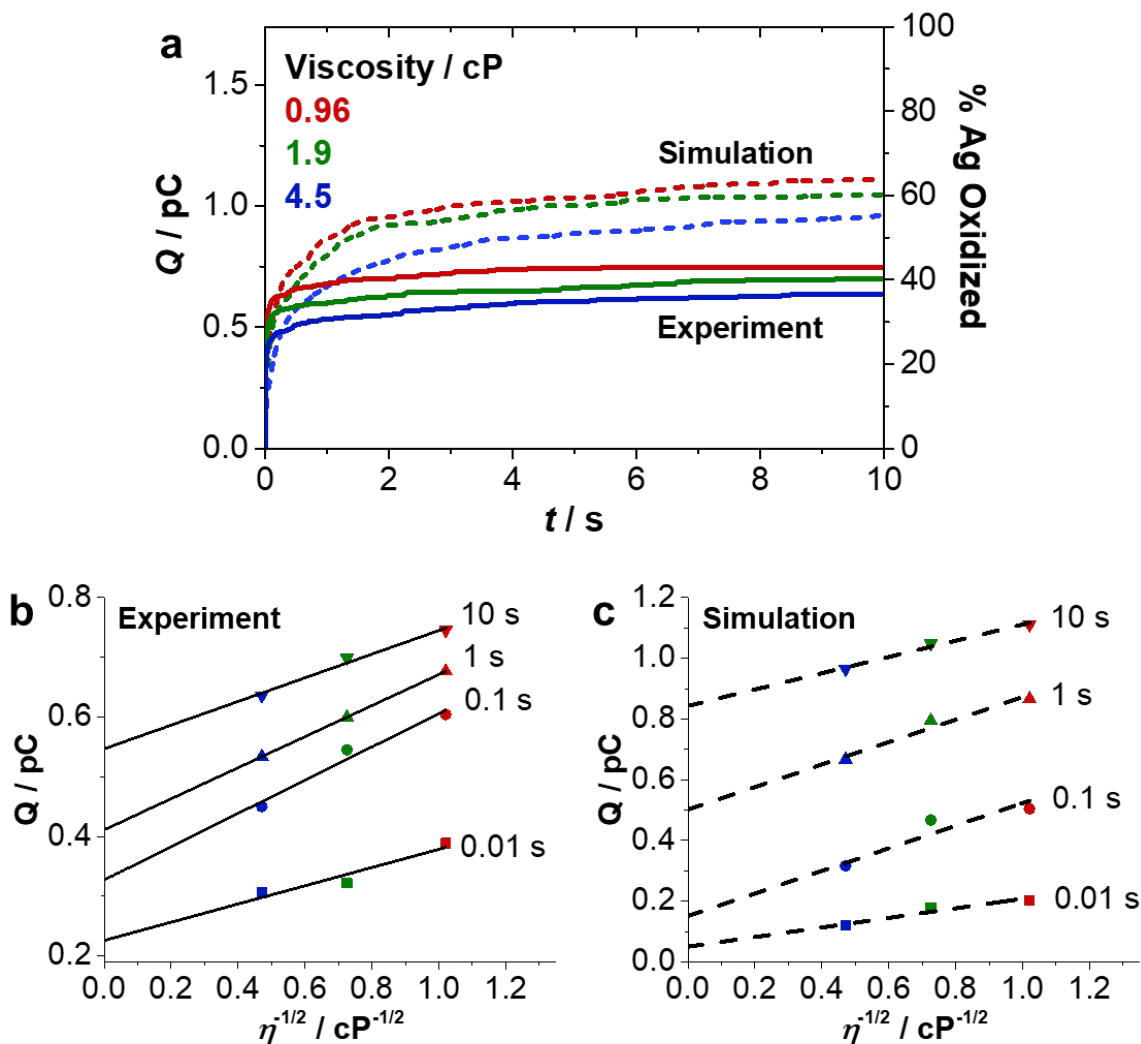


Figure S11. a) Moving average of the Ag oxidation cumulative charge, Q , over time for a single Ag nanoparticle as acquired from experiment (solid lines) and simulation (dashed lines). The colors of the plots in are coded to viscosity: red, 0.96 cP; green, 1.90 cP; blue, 4.51 cP. Details for construction of the experimental Q vs t plot are provided in section S9. Average cumulative Q at $t = [10, 1, 0.1, \text{ and } 0.01 \text{ s}]$ plotted as a function of $\eta^{-1/2}$ for both b) experiment and c) simulation with dashed lines resulting from linear fits. Results were averaged from the same sample population of single-particle measurements, N_{NP} , listed in Table 1 of the main text and plot on a shorter time scale in Figure 7.

S13. References

- (1) Cheng, N.-S. Formula for the Viscosity of a Glycerol–Water Mixture. *Ind. Eng. Chem. Res.* **2008**, *47*, 3285-3288.
- (2) Rees, N. V.; Zhou, Y.-G.; Compton, R. G. The Aggregation of Silver Nanoparticles in Aqueous Solution Investigated Via Anodic Particle Coulometry. *ChemPhysChem* **2011**, *12*, 1645-1647.
- (3) Kleijn, S. E. F.; Serrano-Bou, B.; Yanson, A. I.; Koper, M. T. M. Influence of Hydrazine-Induced Aggregation on the Electrochemical Detection of Platinum Nanoparticles. *Langmuir* **2013**, *29*, 2054-2064.
- (4) Robinson, D. A.; Kondajji, A. M.; Castañeda, A. D.; Dasari, R.; Crooks, R. M.; Stevenson, K. J. Addressing Colloidal Stability for Unambiguous Electroanalysis of Single Nanoparticle Impacts. *J. Phys. Chem. Lett.* **2016**, *7*, 2512-2517.
- (5) Oja, S. M.; Robinson, D. A.; Vitti, N. J.; Edwards, M. A.; Liu, Y.; White, H. S.; Zhang, B. Observation of Multiplexed Collision Behavior During the Electro-Oxidation of Single Ag Nanoparticles. *J. Am. Chem. Soc.* **2017**, *139*, 708-718.
- (6) Diaz-Morales, O.; Calle-Vallejo, F.; de Munck, C.; Koper, M. T. M. Electrochemical Water Splitting by Gold: Evidence for an Oxide Decomposition Mechanism. *Chem. Sci.* **2013**, *4*, 2334-2343.
- (7) Chen, Y.; Li, C. W.; Kanan, M. W. Aqueous CO₂ Reduction at Very Low Overpotential on Oxide-Derived Au Nanoparticles. *J. Am. Chem. Soc.* **2012**, *134*, 19969-19972.
- (8) Min, X.; Chen, Y.; Kanan, M. W. Alkaline O₂ Reduction on Oxide-Derived Au: High Activity and 4e⁻ Selectivity without (100) Facets. *Phys. Chem. Chem. Phys.* **2014**, *16*, 13601-13604.
- (9) Bard, A. J.; Faulkner, L. R. *Electrochemical Methods: Fundamentals and Applications, 2nd Ed.*; Wiley: New York; 2001.
- (10) Zhang, F.; Defnet, P. A.; Fan, Y.; Hao, R.; Zhang, B. Transient Electrocatalytic Water Oxidation in Single-Nanoparticle Collision. *J. Phys. Chem. C* **2018**, *122*, 6447-6455.
- (11) Robinson, D. A.; Edwards, M. A.; Ren, H.; White, H. S. Effects of Instrumental Filters on Electrochemical Measurement of Single-Nanoparticle Collision Dynamics. *ChemElectroChem* **2018**, *5*, 3059-3067.